SUPPLEMENTARY INFORMATION

Section 1: Materials and Methods

Vesicle preparation: 2 types of lipid compositions were used: **1)** soy-bean polar lipid extract (SPE, 99% w/w) (Avanti Polar Lipids) and Texas Red/1,2-dihexadecanoyl- sn-glycero-3 phosphoethanolamine triethylammonium salt (TR-DHPE 1% w/w) (natural plasma membrane extract consisting of representative types of lipids) and **2)** soy phosphatidic acid (Soy PA, 15% w/w), soy phosphatidyl choline (Soy PC, 59% w/w), soy phosphatidyl inocitol (Soy PI, 25%), 1% TR-DHPE (artificial mixture of lipids, enriched in phosphatidyl choline (zwitterionic), which is one of the most dominant species in all plasma membranes, doped with PI and PA lipids, which add negative charge to PC, to accomplish effective Ca^{2+} binding). The pore repair behavior of these two different lipid compositions is indistinguishable. 3 ml of a lipid-dye suspension (10 mg/ml) were prepared for each mixture[1]. 3 µl of each suspension were dehydrated for 15 min on a cover slip in an evacuated desiccator. The dry lipid films were subsequently rehydrated with 1 ml of 10 mM HEPES buffer (contains only 10 mM HEPES and 100 mM NaCl, pH 7.8 adjusted with NaOH, Sigma) for 10 min to allow formation of multilamellar vesicles (MLVs). MLV samples were transferred into an observation chamber with a SiO_2 coated cover slip at the bottom, containing 5 ml of 10 mM HEPES buffer with 4 mM $CaCl_2$. After MLVs spread and ruptures appeared, the buffer solution containing 10 mM HEPES, 100 mM NaCl, 10 mM BAPTA (pH=7.8 adjusted with NaOH) was slowly injected into the observation chamber via an automatic pipette. By the same means the ambient buffer containing 4 mM Ca^{2+} was removed. Deionised water was obtained from a Milli-Q system (Millipore).

Surface fabrication: Glass cover slips (Menzel Gläser) were pre-cleaned by sonication in presence of Microposit remover 1165 (Shipley) and oxygen plasma treated at 250W for 2 min in a microwave plasma (Tepla Plasma Batch System 300, AMO GmbH). SiO_2 was deposited onto the cleaned glass substrate by reactive sputtering, using a MS 150 Sputter system (FHR Anlagenbau GmbH), to a final film thickness of 84 nm. Surface quality was confirmed by contact angle measurements (contact angle with water between 0 and 5). All steps of fabrication were performed in the clean room facility MC2, at Chalmers University of Technology.

Microscopy imaging: An inverted microscope (Leica DM IRB, Wetzlar, Germany, equipped with a Leica PL Fluotar 10x/0.30 PH 1 objective, was used for imaging. Texas Red DHPE was excited at 532 nm by a solid state laser (MGL-III-532, Changchun New Industries, Changchun, China). A Chameleon USB camera (Point Gray Research Inc., Richmond, Canada) was used with Fly Capture SDK software to collect the images. Time series were recorded with 2 frames/min.

Data analysis: The dynamics of wetted areas were analyzed from the fluorescent image series using ImageJ (NIH). The pore edge contours and pinning points were determined with Adobe Photoshop CS4 extended. Image overlays were created with Adobe Illustrator CS4 (Adobe Systems, Mountain view, CA).

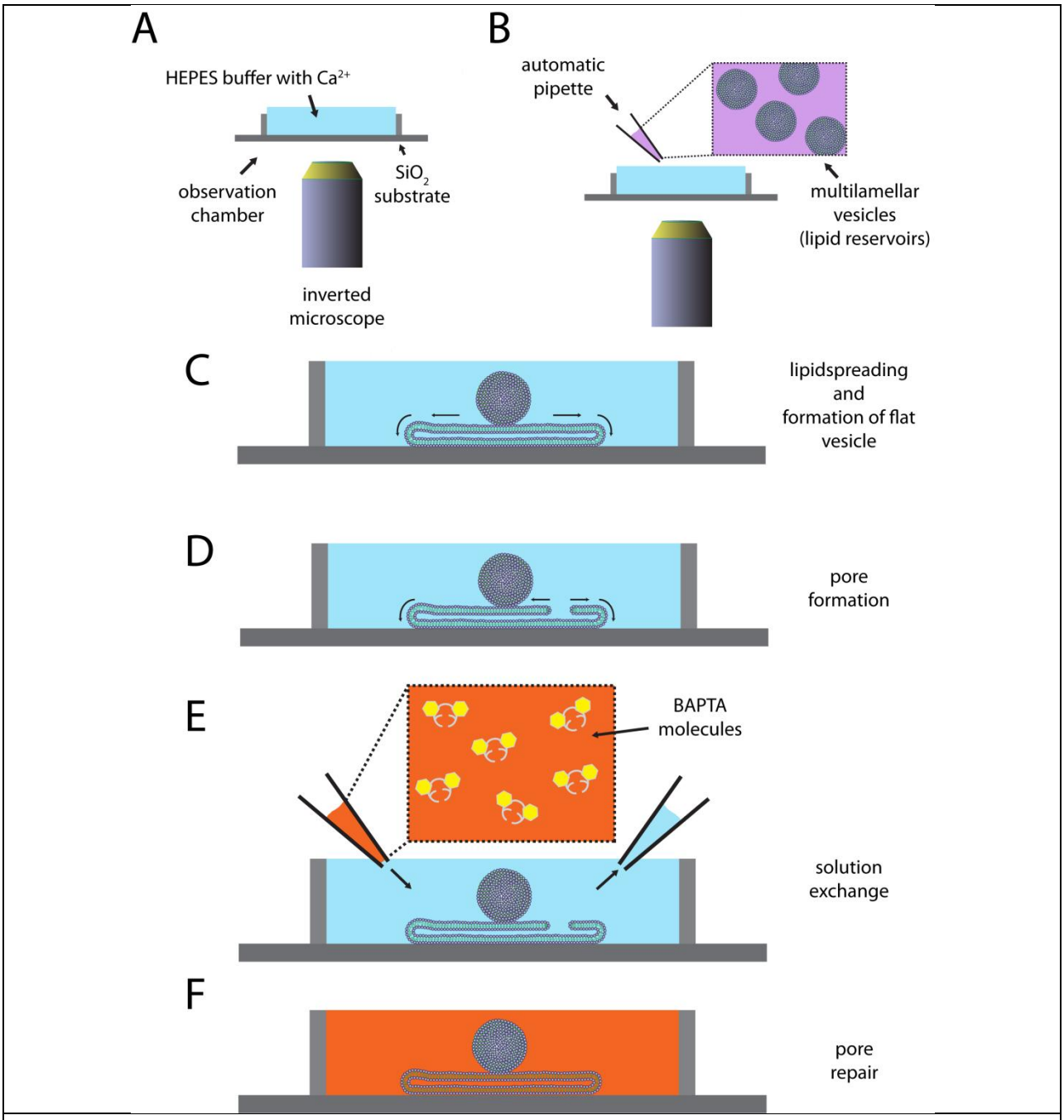

Figure S1. Experimental setup and procedure. (A) Experimental setup. The observation chamber consist of a SiO_2 coated glass substrate, and aqueous HEPES buffer containing Ca^{2+}. Observations are made by means of an inverted laser induced fluorescence (LIF) microscope. (B) The MLV suspension is added to the observation chamber by means of an automatic pipette. (C) The MLVs adhere onto the substrate, start spreading and form the flat giant unilamellar vesicle. (D) Continious spreading causes inscreased tensile stress in the membrane, which results in pore opening. (E) The Ca^{2+} containing buffer is removed while buffer with Ca^{2+}-chelators is added. (F) The chelators remove the Ca^{2+} pinning sites at the pore edges and repair the membrane.

Section 2: Substrate Topography

We have performed scanning probe microscopy (SPM) (Veeco Dimension ICON SPM) in tapping mode using a TESPA Probe (Bruker AFM Probes, Camarillo, CA) on the 84 nm thick SiO_2 to reveal the surface structure on the nanometer scale.

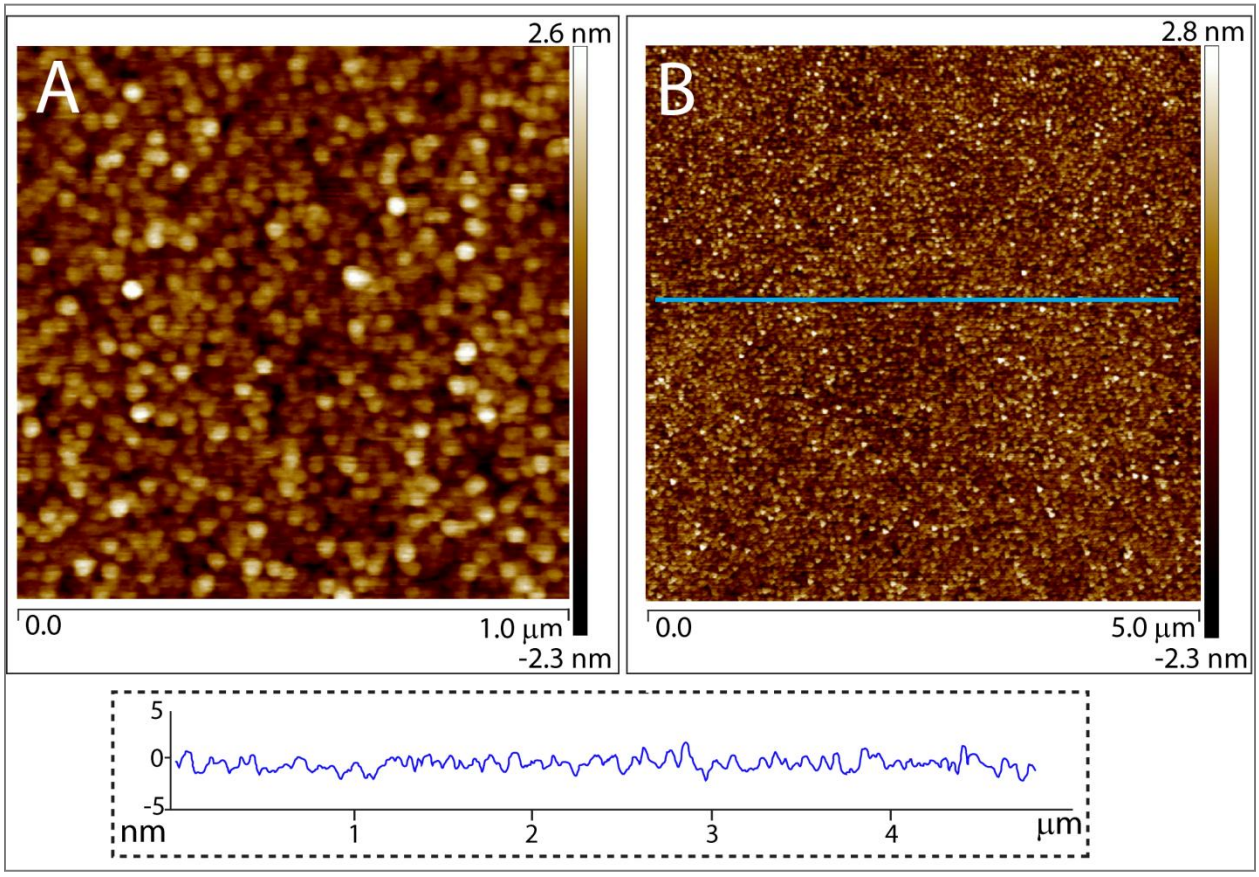

Figure S2: The scanning probe microscopy (SPM) images of a substrate with a SiO_2 film thickness of 84 nm. (A) SP micrograph of a 1 x 1 µm region. **B)** SP micrograph of a 5 x 5 µm region. Inset shows the topography profile along the blue line in **(B)**. Using NanoScope Analysis Software 1.20 (Veeco), images in **(A)** and **(B)** have been flattened; image in **(A)** has been median filtered (3x3).

Section 3: Three Dimensional (3D) Intensity Plots of Pore Regions

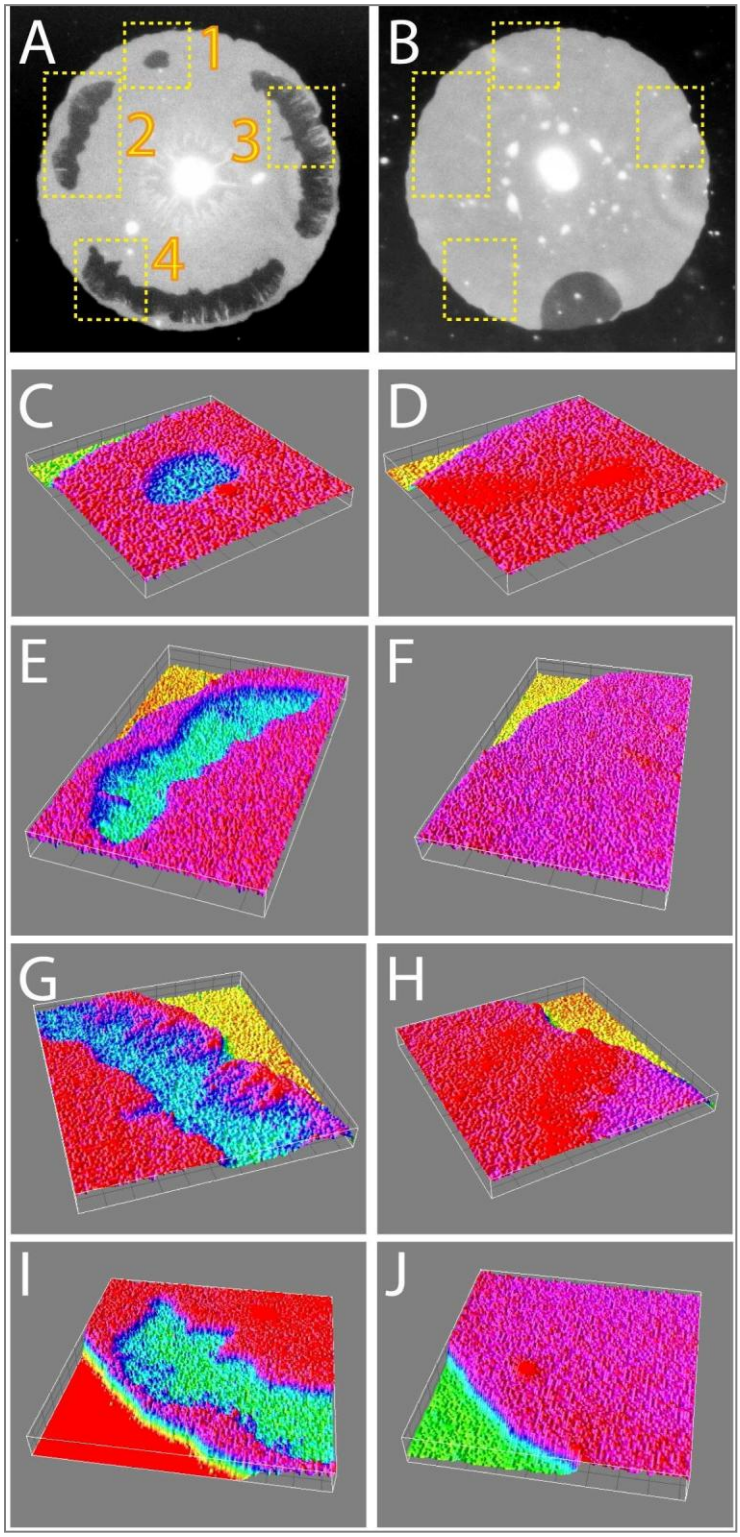

Using Image J (NIH), we have constructed 3D plots of 4 regions of interests (ROIs) based on the fluorescent intensity, before and after pore closure.

Figure S3: Three dimensional intensity plots of pore regions. (A and **B**) 3D Fluorescent micrographs of the flat vesicle in Figure 1 of the main article before and after the pore closure, respectively. The numbers in (**A)** is defines the regions of interest. (**C-J)** The 3D constructions of the regions of interest. Left columns reveal the structures of pores and right columns visualize the corresponding region of the healed membrane after the pore closure. (**C-D)**, (**E-F)**, (**G-H)** and (**I-J)** represent the ROIs #1,2,3,4; respectively. The fractions on the right panels reveal the healed membrane regions with no open pore remaining (pixel dimensions 500 x 500nm).

Section 4: Auxiliary and Control Experiments

1-Figure S3 (A-E): We have performed a control experiment, in which we replaced 10 mM BAPTA buffer with 10 mM HEPES buffer (free of Ca^{2+} and BAPTA). We observed that the rupture propagation did not stop immediately, as it does if BAPTA buffer is applied. The ruptures progressed rapidly to bigger pores. This is an anticipated result, since membrane- and surface-bound Ca^{2+} is only slowly depleted by release into the calcium-free solution. The remaining surface-bound Ca^{2+} resulted in further spreading and rupturing of the flat vesicles.

2-Figure S3 (F-I): We performed a second set of buffer exchange experiments in order to completely remove the surface bound Ca^{2+}, which immediately halted further spreading and allowed investigating the pore development under BAPTA-free and Ca^{2+}-free conditions. We exchanged first with 10 mM BAPTA and then rapidly with 10 mM HEPES buffer (free of Ca^{2+} and BAPTA). Under these conditions, Ca^{2+} inside the pore edges would remain, since diffusion within the nanosized inter-bilayer gap is expected to be slow. We observed the much delayed closure of small pores (5-10 µm). Large pores with dimensions of a few hundred micrometers only shrunk in size but remained open, and eventually even enlarged.

3-Figure S3 (J-N): A structurally modified Ca^{2+}-chelator, Calcium Green™-1, as membrane-impermeant hexapotassium salt (Invitrogen, Excitation: 488 nm, Emission:500-600 nm) was applied instead of BAPTA. Calcium Green™-1 is a BAPTA derivative, carrying a bulky side group which exhibits Ca-dependent fluorescence emission. First the initial buffer (4 mM Ca^{2+} in 10 mM HEPES) was exchanged to 10 mM HEPES (free of Ca^{2+} and BAPTA) to remove free Ca^{2+} from the solution. Then, we rapidly exchanged the ambient solution to 20 µM Ca-green in 10 mM HEPES buffer. Similar to the application of BAPTA, we observed rapid closure of large area pores.

4-Figure S3 (S-T): In order to investigate if the pore closure is reversible, we have performed a combination of 2 and 3, with subsequent calcium addition (*cf.* Table 1). 5 µM Ca-green in 10 mM HEPES was used. After we had observed pore shrinkage, we added 0.5 mM Ca^{2+}. As anticipated, the pores enlarged again, due to continuing (Ca^{2+} induced) spreading of the flat vesicle. We note that no fluorescence signal could be associated with calcium binding. This is expected, as the total amount of calcium within a FGUV, even under the most favorable conditions (200 µm FGUV diameter, 100 nm inter-bilayer water layer, 10 mM internal concentration), is only around 30 femtomoles. That amount is further reduced by rupture/pore formation.

Table 1. Buffer exchange sequences.

#	Initial buffer	Exchanged to	Observations	Figures
1	4 mM Ca^{2+}	0 mM Ca^{2+}	Further spreading and rupturing of the lipid patch	Figure S3 (A-E)
2	4 mM Ca^{2+}	10 mM BAPTA, *then* 0 mM Ca^{2+}	Closure of micrometer-sized pores within several hours. Shrinking of large pores within 160 minutes, then enlargement.	Figure S3 (F-I)
3	4 mM Ca^{2+}	0 mM Ca^{2+}, *then* Ca-Green (20 µM in HEPES)	Rapid closure of micrometer-sized pores	Figure S3 (J-N)
4	4 mM Ca^{2+}	10 mM BAPTA, *then* 0 mM Ca^{2+}, *then* Ca-Green (5 µM in HEPES), *then* 0.5 mM Ca^{2+}	Partial closure of micrometer-sized pores, continuing pore enlargement after final calcium addition	Figure S3 (O-T)

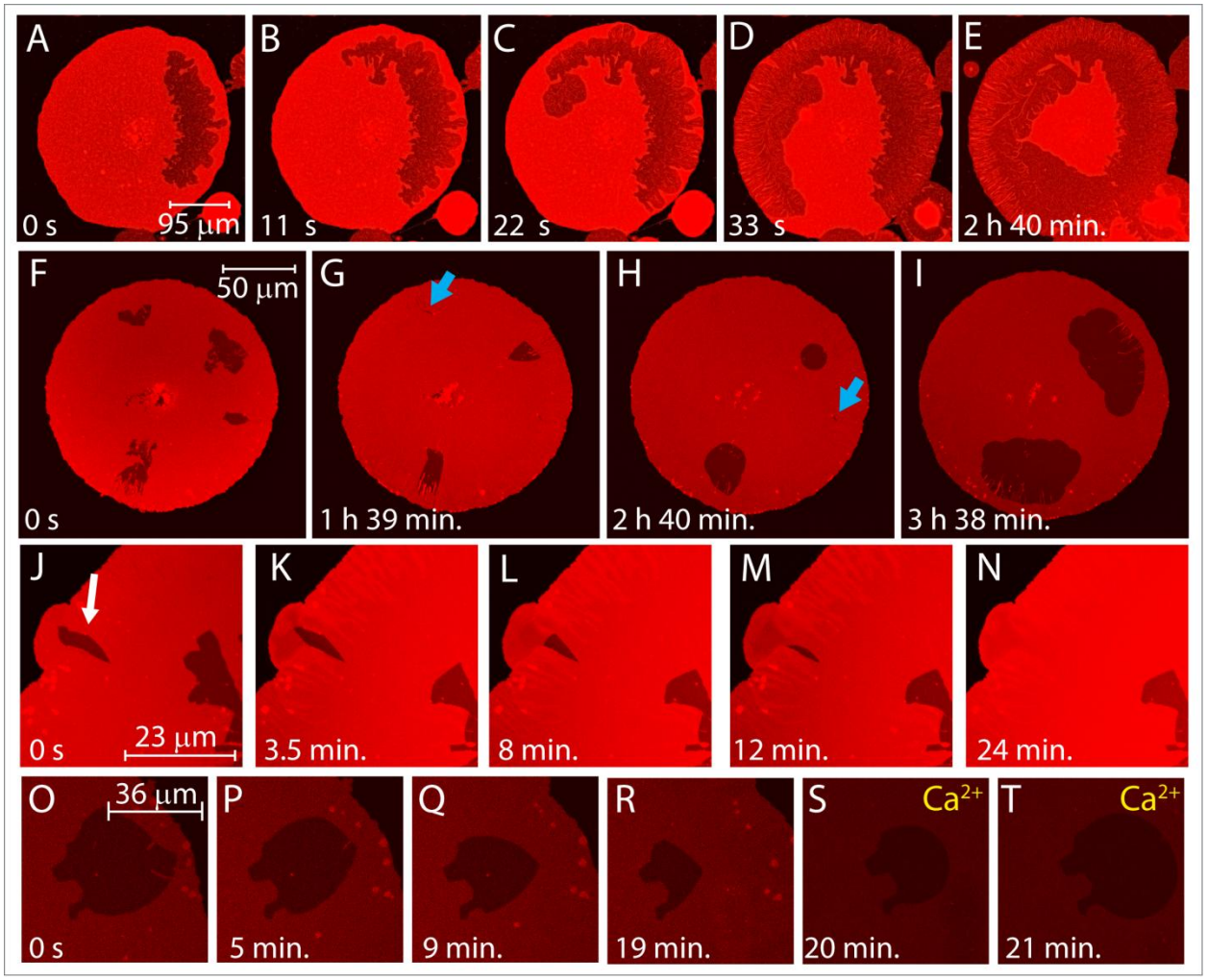

Figure S4: Experiments showing the impact of chelators/ions in the pore healing mechanism of flat vesicles. Imaging of all panels was performed using confocal laser scanning microscopy (Leica TCS SP2 RS with 40x oil objective). Lipid membranes (PC-PI-PA mixture as described in the main article) were doped with 1% Texas-Red DHPE (Invitrogen, Excitation: 594 nm, Emission: 600-700 nm). **(A-E)** Control experiments showing the impact of BAPTA in the pore healing process. The ambient solution is exchanged to 10 mM HEPES (free of Ca^{2+} and BAPTA) instead of 10 mM BAPTA solution. The vesicle continues to spread and the pore propagates. **(F-I)** Experiments showing the pore healing in 10 mM HEPES solution, subsequent to the rapid flushing of the observation chamber with 10 mM BAPTA. In this conditions pore healing (of small pores, shown by blue arrows) can be achieved with much slower rates. Bigger pores enlarge after very long waiting times. **(J-N)** Resealing of a small size pore (white arrow in J) is achieved with another chelator Ca-green. **(O-T)** Resealing (O-R) and enlarging (S-T) of a pore due to Ca-green chelation and Ca^{2+} addition, respectively.

Section 5: Calculation of the dissipation due to the monolayer sliding friction (For Fig.3)

We calculate the monolayer sliding friction using a dissipation fuction for a case where the pore edge has no direct connection to the lipid reservoir (MLV) via the distal (upper) bilayer membrane, i.e., membrane flow occurs exclusively through the proximal (lower) bilayer membrane.

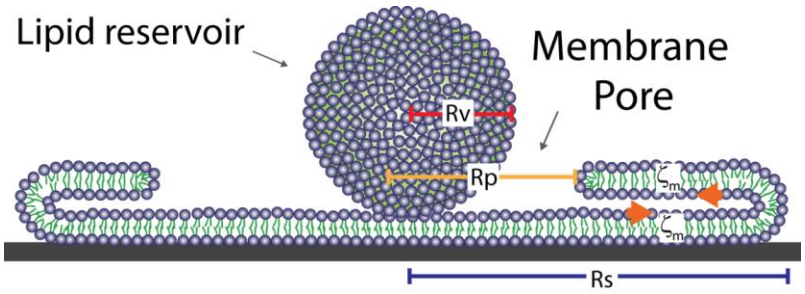

Figure S5. Schematic of the pore closure mechanism of the vesicle in Fig.3 of the main article. R_v, R_p and R_s stand for the radius of the multilamellar vesicle, the radius of the pore and the radius of the spread patch; respectively. ζ_m is the friction coefficient for sliding friction between the leaflets within the proximal and distal bilayers.

$T\dot{S}$ = Dissipation due to sliding friction

R_s = Radius of the spread

R_p = Pore radius

R_L = Effective radius of the lipid source ($R_L \sim R_V$)

ζm = Coefficient of monolayer sliding friction (sliding friction between the leaflets of the bilayer)

v = Velocity of the sliding monolayer

γ = Pore edge tension

E = Line tension energy of the pore

$T\dot{S} = \int_I dA \frac{1}{2}\zeta_m v_I^2 + \int_{II} dA \frac{1}{2}\zeta_m v_{II}^2$ (I and II refer to surface area of the prox. and dist. bilayers, respectively)

$= \int_{R_L}^{R_S} 2\pi r dr \frac{1}{2}\zeta_m (2\frac{Rp\dot{R}p}{r})^2 + \int_{R_p}^{R_S} 2\pi r dr \frac{1}{2}\zeta_m (2\frac{Rp\dot{R}p}{r})^2$ $\dot{R}_p = dR_p/dt$

$= 4\pi\zeta_m R_p^2 \dot{R}_p^2 \ln(\frac{{R_s}^2}{R_L R_p})$

$\dot{E} = 2\pi\gamma\dot{R}_p$

=> $2\frac{\zeta_m R_p^2}{\gamma}\dot{R}_p \ln(\frac{{R_s}^2}{R_L R_p}) = 1$

Time to close a pore with radius R_p: $\tau \backsim \frac{\zeta_m R_p^3}{\gamma}$

$\tau \sim 90$ min

$R_p \approx 50$ µm

Pore edge tension= 10^{-11} N (Reference 2)[2]

$$\zeta_m = \frac{90*60*10^{-11}}{50^3*10^{-18}} \backsim 10^5 - 10^6 \text{ N*s/m}^3$$

The typical values for the monolayer (inter-leaflet) sliding friction coefficients have been previously reported to be 10^8-10^9 Ns/m^3[3, 4]. Those values are significantly higher than the coefficients we estimate. Bilayer sliding in pinning-free regions of the proximal bilayer might complement inter-leaflet sliding to some extent. However, simulation studies have shown that the inter-leaflet monolayer sliding friction can be eased down to 10^6 Ns/m^3[5] depending on morphology of lipids constructing the bilayer. Therefore we do not completely rule out the possibility of pore closure via monolayer sliding. We note that the above calculation assumes a continuous pore closure process, which is not necessarily the case. Sequential de-pinning could delay continuous pore closure, which would make monolayer sliding even less likely.

Section 6: Calculation of the dissipation due to the bilayer sliding friction

(For Fig.2)

We now calculate the bilayer sliding frictional dissipation, in case the distal(upper) bilayer membrane is directly connected to the lipid reservoir (MLV). We consider a simple model for pore closure in a radial flow geometry.

ζ = the sliding friction coefficient between the distal and the proximal bilayers.

v = Velocity of the sliding bilayer.

R_c = Cut off characteristic length scale (R_C~R_S).

$T\dot{S} = \int dA \frac{1}{2}\zeta v^2 = \pi\zeta R_p^2 \dot{R}_p^2 \ln(\frac{R_c}{R_p})$

$\dot{E} = 2\pi\gamma\dot{R}_p$

$R_p \sim 30$ µm

Neglecting logarithmic corrections give:

$\Rightarrow \tau \sim \frac{\zeta R_p^3}{\gamma}$

$\tau_{experimental}$ ~600 seconds (We consider the duration in Fig. 2 (I-J), when the pore closure is not governed by de-pinning.)

$$\zeta = \frac{600.10^{-11}}{30^3 10^{-18}} \sim 10^5 \text{ N*s/m}^3$$

$$\zeta = \frac{\eta}{d}$$ (Reference 6)[6]

d= Thickness of the lubricating water layer between the two membranes.

η = Water viscosity.

$\frac{\eta}{d} = 2.10^5 \frac{Ns}{m^3}$ =>>> $\eta = 10^{-3} \frac{Ns}{m^2}$ d=$\frac{10^{-3}}{2.10^5}$ =∽ $5\ nm$

The result is in the same order of magnitude as the previously estimated value for the lubricating water layer for bilayer sliding[6].

Section 7: Three Dimensional (3D) Intensity Plots of Thin Lipid Structures Inside the Pores

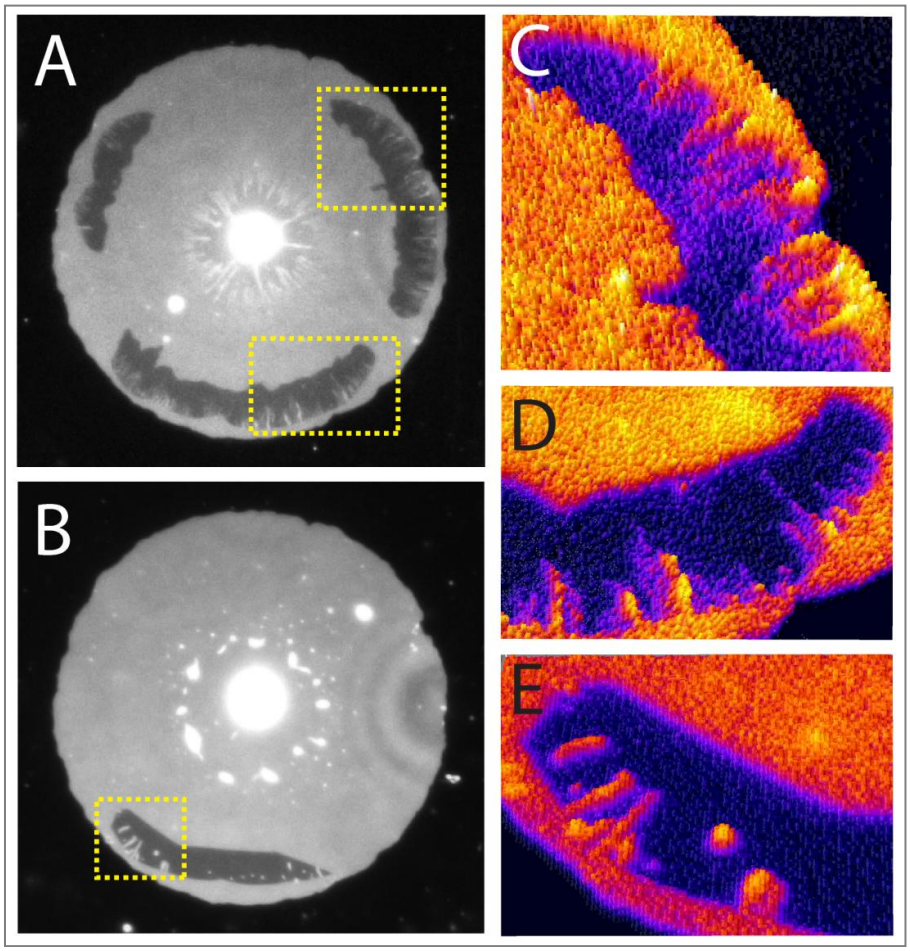

Figure S6: 3D fluorescence intensity plots of thin lipid structures (ImageJ, NIH). (**A** and **B**) 2D Fluorescence micrographs of the flat vesicle in Figure 1(B) and 1(E) of the main article. (C-E) are magnifications of the yellow-framed regions in (A) and (B) to accentuate the thin lipid structures in the pore regions.

References

1. Karlsson, M.; Nolkrantz, K.; Davidson, M. J.; Stromberg, A.; Ryttsen, F.; Akerman, B.; Orwar, O., *Anal. Chem.* **2000,** *72* (23), 5857-5862.
2. Sandre, O.; Moreaux, L.; Brochard-Wyart, F., *Proc. Natl. Acad. Sci. U. S. A.* **1999,** *96* (19), 10591-10596.
3. Shkulipa, S. A.; Den Otter, W. K.; Briels, W. J., *Phys. Rev. Lett.* **2006,** *96* (17).
4. Czolkos, I.; Erkan, Y.; Dommersnes, P.; Jesorka, A.; Orwar, O., *Nano Lett.* **2007,** *7* (7), 1980-1984.
5. Den Otter, W. K.; Shkulipa, S. A., *Biophys. J.* **2007,** *93* (2), 423-433.
6. Rädler, J.; Strey, H.; Sackmann, E., *Langmuir* **1995,** *11* (11), 4539-4548.